LA-UR-15-23625
Approved for public release; distribution is unlimited.

Title: Effect of point defects on the thermal conductivity of UO2: molecular dynamics simulations

Author(s): Liu, Xiang-Yang
Stanek, Christopher Richard
Andersson, Anders David Ragnar

Intended for: Report

Issued: 2015-07-21 (rev.1)

Effect of point defects on the thermal conductivity of UO_2: molecular dynamics simulations

X.-Y. Liu, C. R. Stanek, D. A. Andersson
Los Alamos National Laboratory, Los Alamos, NM 87545

The thermal conductivity of uranium dioxide (UO_2) fuel is an important materials property that affects fuel performance since it is a key parameter determining the temperature distribution in the fuel, thus governing, e.g., dimensional changes due to thermal expansion, fission gas release rates, *etc.* [1] The thermal conductivity of UO_2 nuclear fuel is also affected by fission gas, fission products, defects, and microstructural features such as grain boundaries. Here, molecular dynamics (MD) simulations are carried out to determine quantitatively, the effect of irradiation induced point defects on the thermal conductivity of UO_2, as a function of defect concentrations, for a range of temperatures, 300 – 1500 K. The results will be used to develop enhanced continuum thermal conductivity models for MARMOT and BISON by INL. These models express the thermal conductivity as a function of microstructure state-variables, thus enabling thermal conductivity models with closer connection to the physical state of the fuel [2].

Computational methods

The non-equilibrium direct method [3-5] is employed in the MD simulations. In this method, a heat current (J) is applied to the system, and the thermal conductivity κ is computed from the time-averaged temperature gradient ($\partial T / \partial z$) from the Fourier's law,

$$\kappa = -\frac{J}{\partial T / \partial z} \quad (1)$$

The thermal conductivity calculations are carried out with the direct method as implemented in LAMMPS package [6]. All atoms in the system are initially assigned Gaussian distributed velocities representing two times of the target temperature. After that, the system is equilibrated for 100 ps in the NVE ensemble so the system relaxes to the target temperature. Then, non-equilibrium MD runs are applied to the system, for a period of 9 – 26 ns. After the thermal equilibration, the initial 4 ns in the thermal

simulation are used to accommodate the transient behavior of the system. After that, the temperature profiles are averaged over the rest of the MD time. The heat control algorithm is based on the method of Jund and Jullien [3]. In this scheme, a fixed amount of energy (ΔE) is added or subtracted from the hot or cold regions by the velocity rescaling at every time step while preserving the total momentum ($\vec{P} = \sum_{i=1,N} m_i \vec{V}_i$) of the atoms in the regions, so that

$$\vec{V}_i^{New} = \vec{V}_i + (1-\alpha)\frac{\vec{P}}{\sum m_i} \tag{2}$$

$$\alpha = \sqrt{1 \pm \frac{\Delta E}{E_k - \frac{1}{2}\sum m_i V_G^2}} \; ; \; V_G = \frac{\left|\vec{P}\right|}{\sum m_i} \tag{3}$$

The original Jund and Jullien algorithm was derived for single species systems. We find that it applies to multiple species systems as well. The heat flux used in the simulations is 1.9 – 3.7 x 10^{-4} eV/nm^2 per time step. To fit the temperature profiles, a least-squares fit for the linear regression is used. The temperature profiles are fitted in the ranges $w < z < L_z/2 - w$, and $L_z/2 + w < z < L_z - w$, where L_z is the length of the simulation supercell in the heat flow direction, with the choice of the excluded width w as 0.13 L_z, as suggested from earlier studies [7]. The obtained gradients from left and right slopes in the temperature profiles are then averaged to determine the thermal conductivity.

The Buckingham type of empirical potential is used to describe the U^{4+} - O^{2-} [8], O^{2-} - O^{2-} [9] interactions in UO_2, as well as the U^{3+} - O^{2-} [10], U^{5+} - O^{2-} [11] interactions. For computational efficiency, the Wolf summation [12] is used to compute the long-range Coulombic interactions. The computational supercells are initially set to the optimized lattice constant 0.5469 nm, with L_z ranging from 19 to 76 nm. For all the simulations, the heat flow direction is in the <100> crystal orientation of UO_2. NPT simulations are carried out to determine the thermal expansions at different temperatures. The thermal expansion strains determined are 0.001865, 0.003803, 0.005827, 0.007905, 0.010089 at 300, 600, 900, 1200, and 1500 K. All thermal conductivity MD simulations are carried out with the thermal expansion taken into account.

In the MD simulations, a fairly significant portion of phonons propagate ballistically through the system due to the significant large phonon mean free path relative to the simulation supercells, but scatter from the hot and cold plates. This causes the thermal conductivity obtained from MD simulations to be lower than they should be, especially at low temperatures. The conventional method to extrapolate the value to an infinitely large system is based on a linear formula,

$$\frac{1}{\kappa} = \frac{1}{\kappa_\infty} + \frac{c}{L_z} \tag{4}$$

where c is a constant related to the scattering by the hot and cold plates, κ_∞ is the thermal conductivity for a simulation cell of infinite length. As shown in our recent work [1], we find that a quadratic correction is sometimes needed in order to take the non-linear effect in the UO_2 lattice into account, which brings the fitting formula to a more general one,

$$\frac{1}{\kappa} = \frac{1}{\kappa_\infty} + \frac{c_1}{L_z} + \frac{c_2}{L_z^2} \tag{5}$$

where c_1 and c_2 are both constants.

Results

We start with results for pure UO_2 before going into the results for point defects. The thermal conductivity for UO_2 obtained from MD simulations at different temperatures using the above methodology is shown in figure 1(a). MD simulations of pure UO_2 are carried out at 300, 600, 900, 1200, and 1500 K. At each temperature, a set of simulations using boxes of different length are performed, 19, 24, 32, 49, and 65 nm, followed by extrapolation according to Eq. 5. We find that long MD simulation times are necessary to provide accurate results for extrapolation to an infinitely large system. For pure UO_2, MD times of 26 ns are used in all simulations. In figure 1(b) MD results for the thermal resistivity κ^{-1} as function of inverse sample length L_z^{-1} for UO_2 at 300 K are shown for several simulation conditions. Due to the stochastic nature of the simulations, even modest long MD simulation time of 10 ns is not enough for pure UO_2 simulations. This is reflected in the changes in the MD data obtained from the three different random processes as shown in Fig. 1(b), as well as the deviation from the 26 ns MD simulation data. The line is a fit to the 26 ns MD data using Eq. 5. From Fig. 1(b), the MD data at

300 K suggests a strong quadratic correction. Also, the extrapolated value to the infinite length, κ_∞, 28.12 W/Km is significantly larger than the MD obtained data, 25.56 W/Km at the largest sample, 65 nm in length.

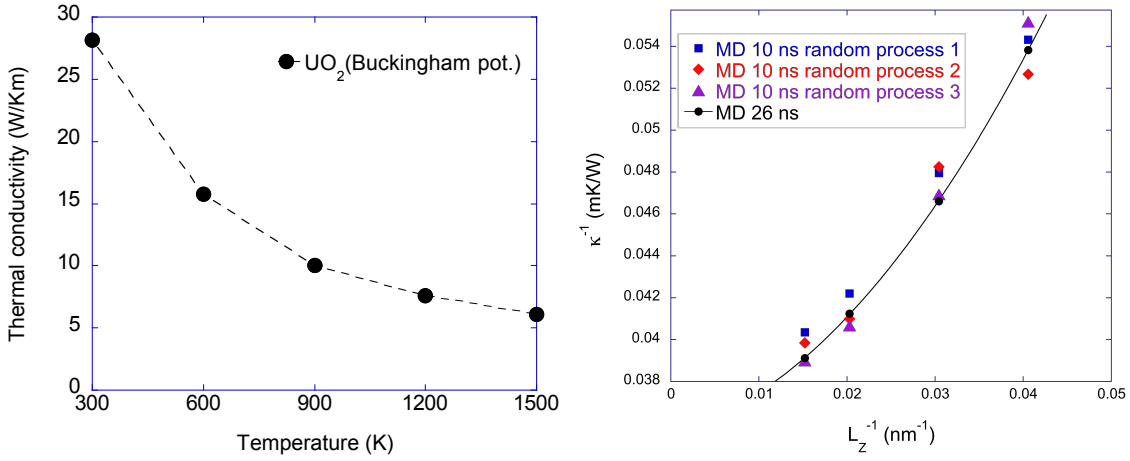

Figure 1. (a) Thermal conductivity for UO_2 at different temperature from MD simulations. (b) MD results for the thermal resistivity κ^{-1} vs. inverse sample length L_z^{-1} for UO_2, at 300 K. The line is a fit to the 26 ns MD data using Eq. 5. The symbols are MD data taken under different simulation conditions.

For point defects, we considered oxygen interstitials (I_O), oxygen vacancies (V_O), uranium interstitials (I_U), and uranium vacancies (V_U). For each V_O or I_U defect, two or four U^{3+} ions are created in the supercell and randomly distributed in order to achieve charge compensation. Similarly, for each I_O or V_U defect, two or four U^{5+} ions are created in the supercell and randomly distributed. We also considered the Schottky trio vacancies in the study, and compared the effect of Schottky defects to that of uranium vacancies.

Figure 2 shows the effect of I_O and V_O on the thermal conductivity of UO_2, as a function of x in UO_{2+x} at different temperatures. The locations of the defect sites are chosen according to a random distribution for the specified composition. The I_O position is in the center of the cubic UO_2 fluorite unit cell, as determined from DFT [13]. Three compositions of oxygen defects, with x = 0.0135, 0.0262, and 0.0397, or 0.67, 1.31, 1.98 atomic percent of I_O (V_O) are introduced to the UO_2 samples. MD simulations are carried out for the UO_2 samples containing oxygen defects at 300, 600, 900, and 1500 K. The sample lengths used to determine the thermal conductivity values are 19 nm, 38 nm, and

57 nm, and in some cases, 76 nm. The impurity scattering from the oxygen defects is fairly strong, leading to a strong decrease in the thermal conductivity at modest temperatures (< 900 K), even for the smallest defect concentrations. The changes in thermal conductivity due to the I_O or V_O defects are approximately the same, suggesting that the impurity scatterings due to these two oxygen defects are similar. At higher temperatures, the reduction of thermal conductivity is smaller, but still shows a clear dependence on the defect concentrations.

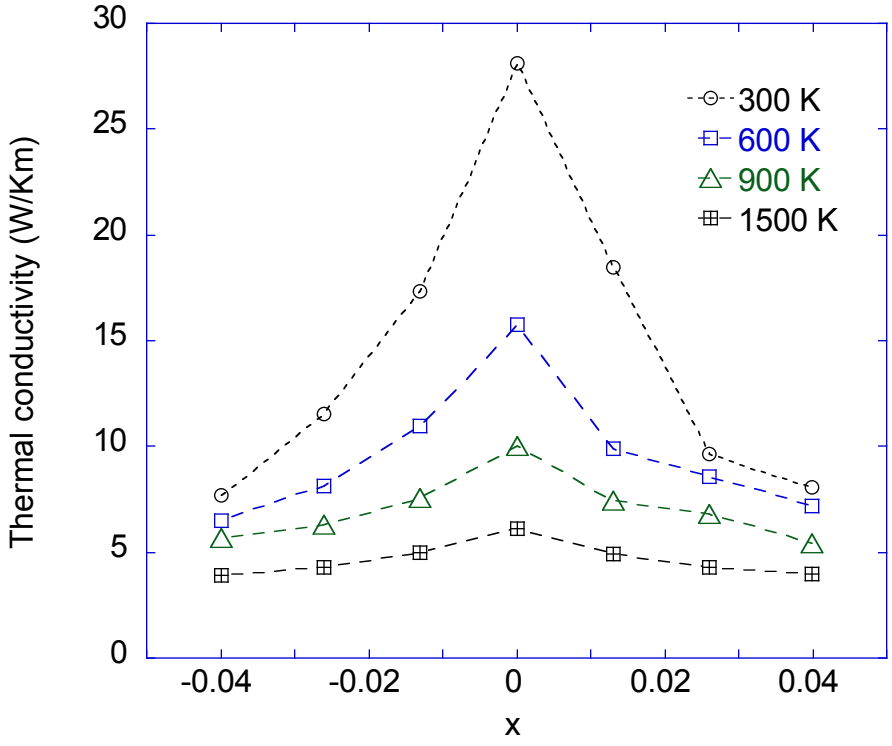

Figure 2. The effect of I_O and V_O defects on the thermal conductivity of UO_2, as a function of x in UO_{2+x} at different temperatures.

Figure 3 shows the effect of I_U and V_U on the thermal conductivity of UO_2, as a function of x in $U_{1+x}O_2$ (the notation used to indicate uranium defects) at different temperatures. The I_U position is also in the center of the cubic UO_2 fluorite unitcell [13]. Two compositions of uranium defects, with x = 0.0135 and 0.0206, or 1.35 and 2.06 atomic percent of I_U (V_U) are introduced to the UO_2 samples. Both MD simulation temperatures and the sample lengths used to determine the thermal conductivity values are similar to the oxygen defect cases. The impurity scattering from the uranium defects

is stronger than the oxygen defect cases for the same x values. Although at the same x value, the concentration of the uranium defects is twice that of the oxygen defects, the total number of uranium defects is the same as that of the oxygen defects for the same simulation supercell, so the comparison for the same x value is still meaningful. The plot in Fig. 3 is slightly asymmetric around x = 0, reflecting that the scattering effect of I_U is slightly stronger (lower thermal conductivity) than that of V_U.

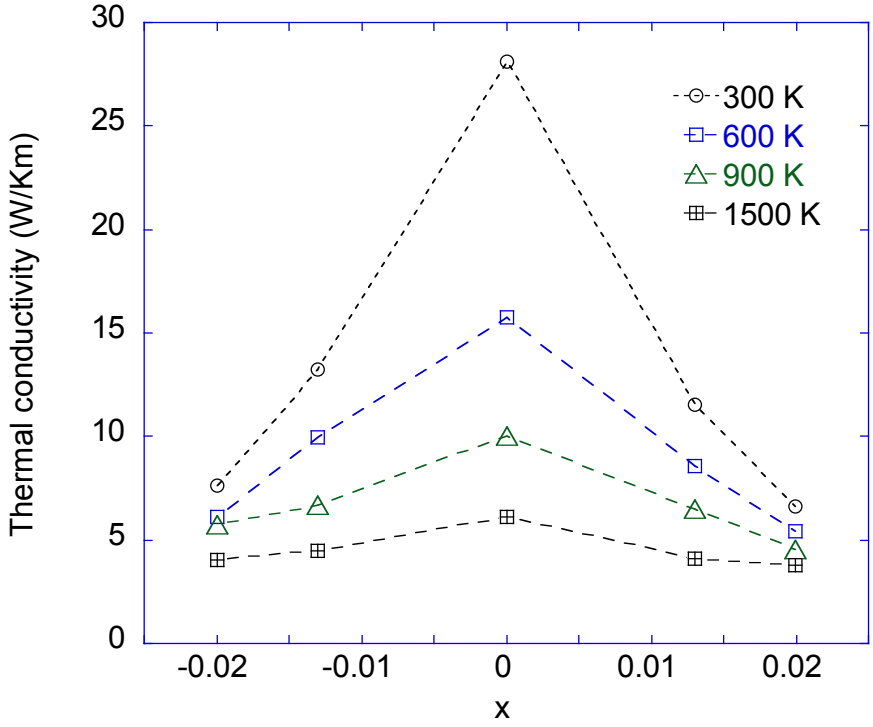

Figure 3. The effect of I_U and V_U defects on the thermal conductivity of UO_2, as a function of x in $U_{1+x}O_2$ at different temperatures.

There are three types of Schottky trivacancy defects in UO_2: with two V_O aligned as nearest neighbors in [100] directions, or with two V_O aligned as next nearest neighbors in [110] directions, or a linear orientation of the O–U–O vacancies along [111] directions. We have chosen the Schottky trivacancy defect with two V_O aligned as next nearest neighbors in [110] directions since this defect configuration is one of the two lowest energy Schottky defect configurations [14-16] and is reported to be the most frequently observed of the three types of Schottky defects formed during displacement cascades [17]. There are two orientations of V_O pairs with respect to the heat flow direction, perpendicular to the direction or non-perpendicular. These two different orientation

configurations are named as V_{sch}^{1} , and V_{sch}^{2}. Figure 4 shows the comparison of the thermal conductivity of V_U and two different orientation configurations of Schottky trivacancy defects in UO_2, in two defect concentrations (x=0.013 and 0.02). From Fig. 4, it is suggested that there is no clear trend which configuration has more impurity scattering than the other configurations. The difference among the thermal conductivities of these different configurations is generally small. In reality the orientation is probably random, but that does not matter if different orientations give rise to the similar scattering.

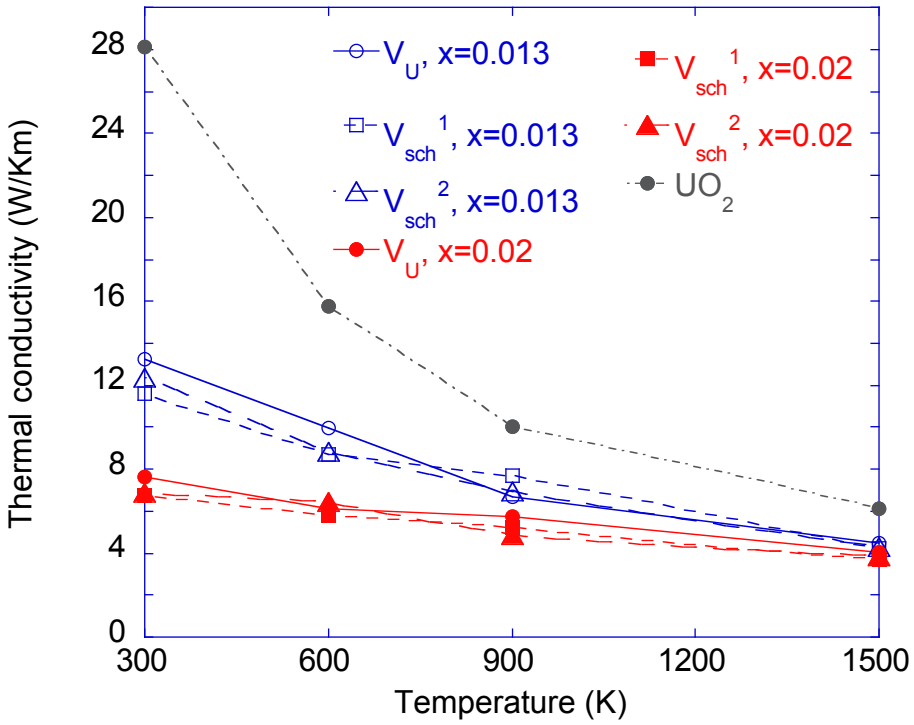

Figure 4. Comparison of the thermal conductivity of UO_2 with V_U defects and UO_2 with two different configurations of Schottky trivacancy defects (V_{sch}^{1} , and V_{sch}^{2}), as a function of temperature, for two defect concentrations (x=0.013 and 0.02). The thermal conductivity of bulk UO_2 is also plotted.

Conclusions

MD simulations have been carried out to determine quantitatively the effect of irradiation induced point defects on the thermal conductivity of UO_2, as a function of defect concentrations, for a range of temperatures, 300 – 1500 K. Allowing long-time MD runs is necessary to provide solid results for extrapolation to an infinitely large

system. The impurity scattering from the oxygen defects is fairly strong, leading to a strong decrease in the thermal conductivity at modest temperatures (< 900 K), even for low defect concentrations. The change of thermal conductivity due to the I_O or V_O defects are approximately the same, suggesting that the impurity scattering due to these two defects are similar. The impurity scattering from the uranium defects is stronger than the oxygen defects. Finally, the differences among the thermal conductivities of UO_2 with uranium vacancy or with various Schottky defects are generally small.

References

[1] K. Gofryk, S. Du, C.R. Stanek, J.C. Lashley, X.Y. Liu, R.K. Schulze, J.L. Smith, D.J. Safarik, D.D. Byler, K.J. McClellan, B.P. Uberuaga, B.L. Scott, D.A. Andersson, Anisotropic thermal conductivity in uranium dioxide, Nature communications, 5 (2014).
[2] M.R. Tonks, P.C. Millett, P. Nerikar, S. Du, D. Andersson, C.R. Stanek, D. Gaston, D. Andrs, R. Williamson, Multiscale development of a fission gas thermal conductivity model: Coupling atomic, meso and continuum level simulations, Journal of Nuclear Materials, 440 (2013) 193-200.
[3] P. Jund, R. Jullien, Molecular-dynamics calculation of the thermal conductivity of vitreous silica, Physical Review B, 59 (1999) 13707-13711.
[4] F. MullerPlathe, A simple nonequilibrium molecular dynamics method for calculating the thermal conductivity, J Chem Phys, 106 (1997) 6082-6085.
[5] T. Ikeshoji, B. Hafskjold, Nonequilibrium Molecular-Dynamics Calculation of Heat-Conduction in Liquid and through Liquid-Gas Interface, Mol Phys, 81 (1994) 251-261.
[6] http://lammps.sandia.gov.
[7] P.C. Howell, Thermal Conductivity Calculation with the Molecular Dynamics Direct Method I: More Robust Simulations of Solid Materials, J Comput Theor Nanos, 8 (2011) 2129-2143.
[8] G. Busker, A. Chroneos, R.W. Grimes, I.W. Chen, Solution mechanisms for dopant oxides in yttria, J Am Ceram Soc, 82 (1999) 1553-1559.
[9] R.W. Grimes, Solution of Mgo, Cao, and Tio2, in Alpha-Al2o3, J Am Ceram Soc, 77 (1994) 378-384.
[10] A.R. Cleave, Atomic Scale Simulations for Waste Form Applications, Ph.D. thesis, Imperial College (2000).
[11] B.E. Hanken, C.R. Stanek, N. Gronbech-Jensen, M. Asta, Computational study of the energetics of charge and cation mixing in U1-xCexO2, Physical Review B, 84 (2011) 085131.
[12] D. Wolf, P. Keblinski, S.R. Phillpot, J. Eggebrecht, Exact method for the simulation of Coulombic systems by spherically truncated, pairwise r(-1) summation, J Chem Phys, 110 (1999) 8254-8282.
[13] X.Y. Liu, D.A. Andersson, B.P. Uberuaga, First-principles DFT modeling of nuclear fuel materials, J Mater Sci, 47 (2012) 7367-7384.
[14] B. Dorado, M. Freyss, G. Martin, GGA plus U study of the incorporation of iodine in uranium dioxide, European Physical Journal B, 69 (2009) 203-209.

[15] A.E. Thompson, C. Wolverton, Pathway and energetics of xenon migration in uranium dioxide, Physical Review B, 87 (2013) 104105.
[16] X.-Y. Liu, D.A. Andersson, Molecular dynamics study of fission gas bubble nucleation in UO2, Journal of Nuclear Materials, 462 (2015) 8-14.
[17] G. Martin, P. Garcia, C. Sabathier, L. Van Brutzel, B. Dorado, F. Garrido, S. Maillard, Irradiation-induced heterogeneous nucleation in uranium dioxide, Phys Lett A, 374 (2010) 3038-3041.